Received: 30 March 2021 | Revised: 28 August 2022 | Accepted: 7 October 2022

DOI: 10.1002/rnc.6440

RESEARCH ARTICLE

WILEY

Time-varying sliding mode controller for over-actuated systems with constrained and uncertain actuators in flight control applications

Seyed Shahabaldin Tohidi[1] | **Yildiray Yildiz**[2] | **Ilya Kolmanovsky**[3]

[1]Department of Applied Mathematics and Computer Science, Denmark Technical University, Lyngby, Kongens, Denmark

[2]Mechanical Engineering Department, Bilkent University, Ankara, Turkey

[3]Department of Aerospace Engineering, University of Michigan, Ann Arbor, Michigan, USA

Correspondence
Seyed Shahabaldin Tohidi, Department of Applied Mathematics and Computer Science, Denmark Technical University, Lyngby, 2800 Kongens, Denmark.
Email: sshto@dtu.dk

Funding information
Turkish Academy of Sciences the Young Scientist Award Program; Türkiye Bilimsel ve Teknolojik Araştirma Kurumu, Grant/Award Number: 118E202

Abstract

One solution to the problem of distributing the control action among redundant actuators with uncertain dynamics is employing an adaptive control allocator. This paper proposes a sliding mode controller which exploits a time-varying sliding surface to complement adaptive control allocation in the presence of actuator saturation. The proposed approach does not require error augmentation for tracking desired references, which diminishes the computational burden. Aero-data Model in Research Environment, which is an over-actuated aircraft model, is adopted to demonstrate the efficacy of the proposed controller in simulation studies.

KEYWORDS

sliding mode controller, control allocation, constrained systems, over-actuated systems

1 | INTRODUCTION

Redundancy in actuators is beneficial for improving functionality and fault tolerance of engineered systems. Such systems require an algorithm to distribute control signals among redundant actuators, which is referred to as control allocation. Systems where control allocation is employed include aircraft/spacecraft,[1-10] marine vessels,[11-16] automobiles,[17-20] robots,[21] and power systems.[22,23]

Control allocation methods can be categorized into the following categories: Pseudo-inverse-based methods, optimization-based methods, and dynamic control allocation. Pseudo-inverse-based control allocation methods[24-27] rely on manipulating the null space of the control input matrix, and have the lowest computational complexity. Optimization-based control allocation methods[28-33] solve an optimization problem at each time instant and can be computationally intense. In dynamic control allocation methods,[34-40] the control signals are distributed among actuators using a set of rules dictated by differential equations. A survey of control allocation methods can be found in Johansen et al.[41] In the presence of actuator uncertainty, the pseudo-inverse and optimization-based control allocation methods require fault detection and identification as well as persistency of excitation assumption for the input signals. Adaptive control

allocation methods[35-37,40] on the other hand, can handle actuator uncertainties without the need for fault identification or persistency of excitation assumption.

Actuator limits can induce nonlinear behavior and lead to performance degradation, limit cycles, multiple equilibria, and even instability.[6,10,32,42] Several control allocation methods have been proposed in the literature that can handle actuator saturation. These include direct control allocation,[24] daisy chaining,[43] pseudo-inverse-based control allocation,[44] and iterative approaches that use the null space of the control input matrix.[27] Optimization-based control allocation is another commonly used method of accounting for actuator magnitude and rate constraints.[1,6,13,28,29,31,45,46] Furthermore, a control allocation approach by Naderi et al.,[47] employs model predictive control to handle actuator magnitude constraints. In order to allocate control signals in the presence of uncertainty as well as actuator constraints, an adaptive control allocator for constrained systems has been developed by Tohidi et al.[38,40] An adaptive control allocator which exploits a modified projection algorithm to handle magnitude and rate constraints in over-actuated systems is proposed by Tohidi et al.[48]

Although control allocation methods enable modularity for the overall control system design, as they separate the generation of the control signal and its distribution, control allocation errors can be significant in transients and degrade the performance. In vehicle and flight applications, the goal of the control allocation is to match the commanded (v) and the actual (Bu) control moments / forces, where u designates a vector of actuator positions. However, the equality $Bu = v$ may not be satisfied in the case of dynamic methods in transients or in the case of optimization-based methods if time to compute the solution online is insufficient. This transient control allocation error may not be negligible especially in the presence of actuator limits. Therefore, the controller must be designed to be robust to the control allocation error, as well as external disturbances. The robustness characteristics of the sliding mode control has motivated its use in combination with many control allocation implementations.[26,49,50]

An approach that employs a sliding mode controller together with a model predictive controller (MPC) has been considered to handle actuator constraints.[51-54] However, this combination leads to high computational complexity due to the need to solve an optimization problem online. Various other sliding mode control approaches have also been proposed which handle the constraints without using MPC.[55-58] However, these methods are developed for single input systems, unlike the one proposed in our paper for over-actuated systems.

Inspired by the work of Corradini et al.,[59] this paper proposes a sliding mode controller with a time-varying sliding surface which guarantees stability and tracking, and which is robust not only to bounded disturbances but also to the adaptive control allocation error. Different from the work of Corradini et al.,[59] the proposed controller solves the tracking problem in over-actuated constrained systems, in the presence of adaptive control allocation transients and disturbances, and in a simpler way by requiring only one design parameter. To the best of the authors knowledge, controllers that are robust to both the adaptive control allocator error and to external disturbances have not been proposed in the prior literature.

The initial results of this study were published in a conference paper by Tohidi et al.[60] Different from the conference version, this paper contains (i) lemma and theorem proofs, (ii) corollaries, detailed discussions and guidance regarding the initial condition selections, (iii) simulation studies demonstrating the robustness of the controller even when sufficient conditions do not hold, and (iv) discussions about the projection algorithm and the control allocation convergence set.

This paper is organized as follows. Section 2 describes the problem of controlling an over-actuated uncertain system in the presence of an adaptive control allocator. Section 3 presents the sliding mode controller design. The ADMIRE model is used in Section 4 to demonstrate the effectiveness of the proposed approach in the simulation environment. Finally, a summary is given in Section 5.

2 | PROBLEM STATEMENT AND PRELIMINARIES

We consider the adaptive control allocation setting in Figure 1 and the following Plant dynamics,[40]

$$\dot{x} = Ax + B_u(\Lambda u + d_u), \tag{1}$$

where $x \in \mathbb{R}^n$ is the state vector, $u = [u_1, \ldots, u_m]^T \in \mathbb{R}^m$ is the actuator input vector whose elements are constrained as $u_i \in [-u_{\max_i}, u_{\max_i}]$, $A \in \mathbb{R}^{n\times n}$ is a known state matrix, $B_u \in \mathbb{R}^{n\times m}$ is a known input matrix and $d_u \in \mathbb{R}^m$ is an unknown

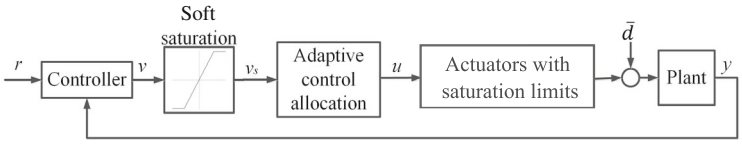

FIGURE 1 Block diagram of the closed loop system

bounded disturbance input. The matrix $\Lambda \in \mathbb{R}^{m\times m}$ is assumed to be diagonal with positive elements representing actuator effectiveness uncertainty. It is assumed that the pair $(A, B_u\Lambda)$ is controllable. Due to actuator redundancy, the input matrix is rank deficient, that is $\text{Rank}(B_u) = \ell < m$. Consequently, B_u can be written as $B_u = B_v B$, where $B_v \in \mathbb{R}^{n\times\ell}$ is a full column rank matrix, that is, $\text{Rank}(B_v) = \ell$, and $B \in \mathbb{R}^{\ell\times m}$. The decomposition of B_u helps exploit the actuator redundancy using control allocation. Employing this decomposition, (1) can be rewritten as

$$\dot{x} = Ax + B_v(B\Lambda u + \bar{d}), \tag{2}$$

where $\bar{d}(t) = Bd_u(t)$ with an upper bound $||\bar{d}(t)|| \le D$, for all $t \ge 0$. Throughout this paper, $||.||$ refers to the Euclidean norm for vectors and induced 2-norm for matrices. The control allocation task is to achieve

$$B\Lambda u + \bar{d} = v_s, \tag{3}$$

where $v_s \in \mathbb{R}^{\ell}$ is the output of the saturation block, which is receiving the control signal v as the input (See Figure 1).

Considering the following dynamics,

$$\dot{y} = A_m y + B\Lambda u + \bar{d} - v_s, \tag{4}$$

where $A_m \in \mathbb{R}^{\ell\times\ell}$ is a stable matrix, a reference model is constructed as

$$\dot{y}_m = A_m y_m. \tag{5}$$

Defining the actuator input as a mapping from v_s to u,

$$u = \theta_v^T v_s, \tag{6}$$

where $\theta_v \in \mathbb{R}^{\ell\times m}$ represents the adaptive parameter matrix to be determined, and substituting (6) into (4), we obtain

$$\dot{y} = A_m y + (B\Lambda\theta_v^T - I_\ell)v_s + \bar{d}, \tag{7}$$

where I_ℓ is an identity matrix of dimension $\ell \times \ell$. It is assumed that there exists an ideal matrix θ_v^* such that

$$B\Lambda\theta_v^{*T} = I_\ell. \tag{8}$$

Defining $e = y - y_m$ and subtracting (5) from (7), it follows that

$$\dot{e} = A_m e + B\Lambda\tilde{\theta}_v^T v_s + \bar{d}, \tag{9}$$

where $\tilde{\theta}_v = \theta_v - \theta_v^*$.

Theorem 1. *Consider (4) and (5). Suppose that the adaptive parameter matrix is updated using the adaptive law,*

$$\dot{\theta}_v(t) = \Gamma_\theta \text{Proj}(\theta_v(t), -v_s(t)e^T(t)PB, f), \tag{10}$$

where the symmetric positive definite matrix P satisfies $A_m^T P + PA_m = -Q$, Q is a symmetric positive definite matrix, "Proj" is the projection operator[48,61] *with a convex function $f \in C^1$, and $\Gamma_\theta = \gamma_\theta I_\ell$, where γ_θ is a positive scalar. Then, given any initial condition $e(0) \in \mathbb{R}^\ell$, $e(t)$ and $\tilde{\theta}_v(t)$ remain uniformly bounded for all $t \geq 0$ and their trajectories converge exponentially to the set*

$$E_1 = \left\{ (e, \tilde{\theta}_v) : ||e||^2 \leq \left(\frac{s\tilde{\theta}_{\max}^2}{\gamma_\theta \lambda_{\min}(Q)} + \frac{2\chi^4 D^2 ||Q||^2}{\sigma^2 \lambda_{\min}(Q)^2} \right) \frac{4s\chi^2 ||Q||}{\sigma \lambda_{\min}(Q)}, ||\tilde{\theta}_v|| \leq \tilde{\theta}_{\max} \right\}, \tag{11}$$

where $s = -\min_i \left(\lambda_i \left(A_m + A_m^T \right)/2 \right)$, $\sigma = -\max_i \left(\text{Real}(\lambda_i(A_m)) \right)$, $\chi = \frac{3}{2}(1 + 4\frac{a}{\sigma})^{(\ell-1)}$, $a = ||A_m||$ and $||\tilde{\theta}_v(t)||_F \leq \tilde{\theta}_{\max} \equiv \sqrt{\sum_{i,j} (\theta_{\max_{i,j}} - \theta_{\min_{i,j}} - \zeta_{i,j})^2}$. In addition, if $\bar{d}(t) = 0$ for $t \geq t'$ for some $t' \geq 0$, and $v_s(t)$ is uniformly continuous as a function of $t \in [t', +\infty)$, then $\lim_{t\to\infty} B\Lambda u(t) = v_s(t)$, that is, (3) is achieved asymptotically.

Proof. See Tohidi et al.[40] ∎

The projection algorithm[48,61] employed in Theorem 1 exploits a continuous function $\text{Proj}(\theta_{v_{i,j}}, Y_{i,j}, f) : \mathbb{R} \times \mathbb{R} \times \mathcal{F} \to \mathbb{R}$ defined as

$$\text{Proj}(\theta_{v_{i,j}}, Y_{i,j}, f) \equiv \begin{cases} Y_{i,j} - Y_{i,j} f\left(\theta_{v_{i,j}}\right) & \text{if } f\left(\theta_{v_{i,j}}\right) > 0 \ \& \ Y_{i,j}\left(\frac{df}{d\theta_{v_{i,j}}}\right) > 0 \\ Y_{i,j} & \text{otherwise,} \end{cases} \tag{12}$$

where $Y_{i,j}$ is equal to $\dot{\theta}_{v_{i,j}}$ before being projected and $f(.) \in \mathcal{F}(\mathbb{R} \to \mathbb{R})$ is a convex and continuously differentiable (C^1) function given as

$$f\left(\theta_{v_{i,j}}\right) = \frac{\left(\theta_{v_{i,j}} - \theta_{\min_{i,j}} - \zeta_{i,j}\right)\left(\theta_{v_{i,j}} - \theta_{\max_{i,j}} + \zeta_{i,j}\right)}{\left(\theta_{\max_{i,j}} - \theta_{\min_{i,j}} - \zeta_{i,j}\right)\zeta_{i,j}}, \tag{13}$$

and where $\zeta_{i,j}$ is the projection tolerance of the (i,j)th element of θ_v, which satisfies $0 < \zeta_{i,j} < 0.5(\theta_{\max_{i,j}} - \theta_{\min_{i,j}})$. $\theta_{\max_{i,j}}$ and $\theta_{\min_{i,j}}$ are the upper and lower bound of the (i,j)th element of θ_v. A step by step method for the determination of the projection bounds is given at Tohidi et al.[40]

By substituting (6) and (8) into (2), it follows that

$$\begin{aligned} \dot{x} &= Ax + B_v\left(B\Lambda u + \bar{d}\right) \\ &= Ax + B_v\left(B\Lambda\theta_v^T v_s + \bar{d}\right) \\ &= Ax + B_v\left(I + B\Lambda\tilde{\theta}_v^T\right)v_s + B_v\bar{d}. \end{aligned} \tag{14}$$

Defining $\Delta B(t) \equiv B\Lambda\tilde{\theta}_v^T(t)$, and substituting in (14), it follows that

$$\dot{x}(t) = Ax(t) + B_v(v_s(t) + d(t)), \tag{15}$$

where $d(t) = \Delta B(t)v_s(t) + \bar{d}(t) \in \mathbb{R}^\ell$ is the sum of the disturbance and the control allocation error. Therefore, the controller to be designed should be robust to both the disturbances and the control allocation errors. It is noted that since $\Delta B(t)$, $v_s(t)$, and $\bar{d}(t)$ are bounded, $d(t)$ is also bounded.

Thus far, we introduced the plant dynamics with constrained uncertain actuators, the adaptive control allocation algorithm, and the resulting system dynamics (15) after the inclusion of the control allocator. What remains to be done is the design of a controller that generates the signal v (see Figure 1). The controller needs to be robust to the control allocation error and the disturbances, in the presence of a software saturation. Note that software saturation is needed for the adaptive control allocator to provide a stable performance. In the proceeding sections, a sliding mode controller that satisfies these requirements is presented.

3 | CONTROLLER DESIGN

In this section, a design procedure for the controller that generates the virtual control signal v is proposed (see Figure 1).

The following two assumptions are made:

Assumption 1. The dynamics in (15) can be written as

$$\begin{bmatrix} \dot{x}^{(1)} \\ \dot{x}^{(2)} \end{bmatrix} = \begin{bmatrix} A_{1,1} & A_{1,2} \\ A_{2,1} & A_{2,2} \end{bmatrix} \begin{bmatrix} x^{(1)} \\ x^{(2)} \end{bmatrix} + B_v(v_s + d), \tag{16}$$

where $A_{1,1} \in \mathbb{R}^{(n-\ell)\times(n-\ell)}$ is a Hurwitz matrix, $A_{1,2} \in \mathbb{R}^{(n-\ell)\times\ell}$, $A_{2,1} \in \mathbb{R}^{\ell\times(n-\ell)}$ and $A_{2,2} \in \mathbb{R}^{\ell\times\ell}$ are parts of the state matrix, and $x^{(1)} \in \mathbb{R}^{(n-\ell)}$ and $x^{(2)} \in \mathbb{R}^{\ell}$ constitute the state vector. It is noted that the elements of the state matrix, $A_{i,j}$, $i = 1, 2$, $j = 1, 2$, are known. We are interested in the vector $x^{(2)}$ as the system output y. Therefore,

$$y = C \begin{bmatrix} x^{(1)} \\ x^{(2)} \end{bmatrix}, \tag{17}$$

where $C = [0_{\ell\times(n-\ell)}\ I_\ell]$.

Assumption 2. The matrix $B_v \in \mathbb{R}^{n\times\ell}$ is in the form $[0_{\ell\times(n-\ell)}\ I_\ell]^T$.

Remark 1. Although the proposed controller can be applied to other dynamical systems satisfying Assumptions 1 and 2, the above assumptions are justified for typical aircraft models,[2,62] which are the main focus of this paper. In the simulation section, these assumptions are validated for the AeroData Model in Research Environment (ADMIRE).[1,29]

Remark 2. For systems where Assumption 2 does not hold, given that B_v has full column rank, it is possible to find a transformation matrix, T_B, such that $\hat{B}_v = T_B B_v = [0_{\ell\times(n-\ell)}\ I_\ell]^T$.[59,63] However, employing this transformation may lead to a state space realization which violates Assumption 1.

Remark 3. Since $A_{1,1}$ is assumed to be Hurwitz, showing that the states $x^{(2)}$ are bounded will be sufficient to demonstrate the boundedness of $x^{(1)}$.

3.1 | Time-varying sliding surface

The sliding surface, inspired by Reference 59, is given as

$$s(x^{(2)}(t), x^{(2)}(t_0), t) = x^{(2)}(t) - x^{(2)}(t_0)e^{-\bar{\lambda}(t-t_0)} - \frac{2}{\pi} r(t)\tan^{-1}(\bar{\lambda}(t - t_0)) = 0, \tag{18}$$

where $\bar{\lambda} > 0$ is a scalar parameter, $x^{(2)} \in \mathbb{R}^{\ell}$ is defined in (16), and $r(t) \in \mathbb{R}^{\ell}$ is the twice continuously differentiable (C^2) reference to be tracked.

The response of a system controlled by a sliding mode controller includes two phases.[64] The first phase is called the reaching phase. During this phase, the controller drives the system towards the sliding surface. In the second phase, which is called the sliding phase, the trajectories evolve on the sliding manifold. For the sliding surface (18), no reaching phase exists since the sliding surface is a function of the initial condition and the trajectories are on the sliding surface at $t = t_0$, that is, $s(x^{(2)}(t), x^{(2)}(t_0), t_0) = 0$. These types of sliding surfaces belong to the family of integral sliding surfaces.[65] Below, we analyze the behavior of the system trajectories on the sliding surface and show that the trajectories remain on the sliding surface for all $t \geq t_0$.

3.2 | Motion on the sliding surface

Using (18), the trajectories of $x^{(2)}$ on the sliding surface satisfy

$$x^{(2)}(t) = x^{(2)}(t_0)e^{-\bar{\lambda}(t-t_0)} + \frac{2}{\pi} r(t)\tan^{-1}\left(\bar{\lambda}(t - t_0)\right). \tag{19}$$

Substituting (19) into (16), it follows that

$$\dot{x}^{(1)} = A_{1,1}x^{(1)} + A_{1,2}\left(x^{(2)}(t_0)e^{-\bar{\lambda}(t-t_0)} + \frac{2}{\pi}r(t)\tan^{-1}\left(\bar{\lambda}(t-t_0)\right)\right). \tag{20}$$

By defining $G_1 \equiv A_{1,2}x^{(2)}(t_0)$, and $G_2(t) \equiv \frac{2}{\pi}A_{1,2}r(t)\tan^{-1}(\bar{\lambda}(t-t_0))$, (20) can be rewritten as

$$\dot{x}^{(1)} = A_{1,1}x^{(1)} + G_1e^{-\bar{\lambda}(t-t_0)} + G_2(t) = A_{1,1}x^{(1)} + g(t), \tag{21}$$

where $g(t) \equiv G_1e^{-\bar{\lambda}(t-t_0)} + G_2(t)$.

Lemma 1. *When $x^{(2)}(t)$ is on the sliding surface (18), $||x^{(1)}(t)|| \leq k\bar{x}^{(1)}(t_0) + K_2\bar{x}^{(2)}(t_0) + K_2\bar{r}$, where $K_2 = \frac{k}{\xi}||A_{1,2}||$, k and ξ are positive constants, and $\bar{x}^{(1)}(t_0)$, $\bar{x}^{(2)}(t_0)$ and $\bar{r}$ are the upper bounds of $||x^{(1)}(t_0)||$, $||x^{(2)}(t_0)||$ and $||r(t)||$, respectively. Furthermore, $\lim_{t\to\infty} y(t) = r(t)$.*

Proof. Per Assumption 1, $A_{1,1}$ is Hurwitz, hence the homogeneous system $\dot{x}_h^{(1)}(t) = A_{1,1}x_h^{(1)}(t)$ is globally exponentially stable at the origin. The solution of this system is given as $x_h^{(1)}(t) = \Phi(t,t_0)x_h^{(1)}(t_0)$, where $\Phi(t,t_0)$ is the state transition matrix and there exist constants $k > 0$ and $\xi > 0$ such that

$$||\Phi(t,t_0)|| \leq ke^{-\xi(t-t_0)}, \quad \forall t \geq t_0, \tag{22}$$

where $\xi = \frac{1}{2||X||}$, $k = \sqrt{||X^{-1}||||X||}$ and the positive definite matrix $X \in \mathbb{R}^{(n-\ell)\times(n-\ell)}$ satisfies the Lyapunov equation $A_{1,1}^TX + XA_{1,1} = -I_{n-\ell}$.[66]

Since the state transition matrices of the dynamics $\dot{x}_h^{(1)}(t) = A_{1,1}x_h^{(1)}(t)$ and $\dot{x}^{(1)}(t) = A_{1,1}x^{(1)}(t) + g(t)$ are the same, we use the state transition matrix $\Phi(t,t_0)$ used in (22) to provide the solution of (21) as

$$x^{(1)}(t) = \Phi(t,t_0)x^{(1)}(t_0) + \int_{t_0}^{t}\Phi(t,\eta)g(\eta)d\eta. \tag{23}$$

Taking the norm of both sides of (23) and using the triangle inequality, we obtain that

$$||x^{(1)}(t)|| \leq ||\Phi(t,t_0)x^{(1)}(t_0)|| + \int_{t_0}^{t}||\Phi(t,\eta)||||g(t)||d\eta. \tag{24}$$

Using the definition of $g(t)$, given after (21), it follows that $||g(t)|| = ||G_1e^{-\bar{\lambda}t} + G_2(t)|| \leq ||G_1|| + \sup_{t\geq t_0}||G_2(t)||$. Note that, since $G_2(t)$ is a function of the reference input $r(t)$, $\sup_{t\geq t_0}||G_2(t)||$ exists (see the definition of G_2 given after (20)). Therefore, $||g(t)|| \leq ||A_{1,2}||\bar{x}^{(2)}(t_0) + ||A_{1,2}||\bar{r}$. Defining $K_1 = ||A_{1,2}||\bar{x}^{(2)}(t_0) + ||A_{1,2}||\bar{r}$, and using (22), (24) can be rewritten as,

$$\begin{aligned}
||x^{(1)}(t)|| &\leq k\bar{x}^{(1)}(t_0)e^{-\xi(t-t_0)} + kK_1\int_{t_0}^{t}e^{-\xi(t-\eta)}d\eta \\
&\leq k\bar{x}^{(1)}(t_0)e^{-\xi(t-t_0)} + kK_1\frac{1}{\xi}\left(1 - e^{-\xi(t-t_0)}\right) \\
&\leq k\bar{x}^{(1)}(t_0) + kK_1\frac{1}{\xi} \\
&= k\bar{x}^{(1)}(t_0) + k\left(||A_{1,2}||\bar{x}^{(2)}(t_0) + ||A_{1,2}||\bar{r}\right)\frac{1}{\xi} \\
&\leq k\bar{x}^{(1)}(t_0) + K_2\bar{x}^{(2)}(t_0) + K_2\bar{r},
\end{aligned} \tag{25}$$

where $K_2 = \frac{k}{\xi}||A_{1,2}||$, and $\bar{x}^{(1)}(t_0)$ and $\bar{x}^{(2)}(t_0)$ represent the upper bounds on $||x^{(1)}(t_0)||$ and $||x^{(2)}(t_0)||$, respectively. Since the reference signal $r(t)$, $x^{(1)}(t_0)$, and $x^{(2)}(t_0)$ are bounded, (25) shows that $x^{(1)}(t)$ is bounded. Since $x(t_0)$ and $r(t)$ are bounded, it can be shown, using (19), that $x^{(2)}(t)$ is bounded and converges to $r(t)$. Since $y = x^{(2)}$, this completes the proof. ∎

3.3 | Control law

Figure 1 shows that once the control signal v is generated by the controller, it is passed through a software saturation block, whose output is represented by v_s. In this subsection, it is assumed that $v_s = v$ to demonstrate that with the proposed control law, trajectories stay on (18) and hence properties of Lemma 1 hold. This requires that v always stays within saturation bounds. A condition for this assumption to hold will be presented in the next subsection.

Definition 1. $\text{sign}_\text{v}(a)$, where a is a column vector, is a diagonal matrix whose elements are the signs of the elements of the vector a. For example, $\text{sign}_\text{v}([a_1\ a_2]^T) = \text{diag}(\text{sign}(a_1),\ \text{sign}(a_2))$, where a_1 and a_2 are scalars.

Definition 2. $|a|_\text{v} \equiv \text{sign}_\text{v}(a)a$ and $|a^T|_\text{v} \equiv a^T\text{sign}_\text{v}(a)$, where a is a column vector and $\text{sign}_v(.)$ is defined in Definition 1. For example, $|[a_1\ a_2]|_\text{v} = [a_1\ a_2]\text{sign}_\text{v}([a_1\ a_2]^T) = [|a_1|\ |a_2|]$, where a_1 and a_2 are scalars.

Theorem 2. *Consider the dynamics in (16) with the control law,*

$$v(t) = -A_{2,1}x^{(1)}(t) - A_{2,2}x^{(2)}(t) - \bar{\lambda}x^{(2)}(0)e^{-\bar{\lambda}t} + \frac{2}{\pi}\dot{r}(t)\tan^{-1}(\bar{\lambda}t) + \frac{2}{\pi}r(t)\frac{\bar{\lambda}}{1+\bar{\lambda}^2t^2} - \text{sign}_\text{v}\left(s(x^{(2)}(t), x^{(2)}(0), t)\right)\rho, \tag{26}$$

where $\rho \in R^r$ contains the absolute upper bounds of the elements of the disturbance vector d, and $s(x^{(2)}(t), x^{(2)}(0), t)$ is the sliding surface (18). Assume $v_s(t) = v(t)$ for all t. Then, the trajectories of $x^{(2)}$ stay on the sliding surface (18).

Proof. Consider a Lyapunov function candidate $V_2(s) = \frac{1}{2}s^Ts$, where the arguments of $s(x^{(2)}(t), x^{(2)}(t_0), t)$ are dropped for clarity. By taking the time-derivative of V_2 along the system trajectories, and using (18) with $t_0 = 0$, we obtain

$$\dot{V}_2 = s^T\dot{s} = s^T\left(\dot{x}^{(2)}(t) + \bar{\lambda}x^{(2)}(0)e^{-\bar{\lambda}t} - \frac{2}{\pi}\dot{r}(t)\tan^{-1}(\bar{\lambda}t) - \frac{2}{\pi}r(t)\frac{\bar{\lambda}}{1+\bar{\lambda}^2t^2}\right). \tag{27}$$

Using (16) and Assumption 2, we have $\dot{x}^{(2)}(t) = A_{2,1}x^{(1)}(t) + A_{2,2}x^{(2)}(t) + v + d$. Therefore, (27) can be rewritten as

$$\dot{V}_2 = s^T\left(A_{2,1}x^{(1)}(t) + A_{2,2}x^{(2)}(t) + v + d + \bar{\lambda}x^{(2)}(0)e^{-\bar{\lambda}t} - \frac{2}{\pi}\dot{r}(t)\tan^{-1}(\bar{\lambda}t) - \frac{2}{\pi}r(t)\frac{\bar{\lambda}}{1+\bar{\lambda}^2t^2}\right). \tag{28}$$

By substituting the control law (26) into (28), and using Definitions 1 and 2, it follows that

$$\dot{V}_2 = s^T[d - \text{sign}_\text{v}(s)\rho] = s^Td - |s^T|_\text{v}\rho \le |s^T|_\text{v}(|d|_\text{v} - \rho). \tag{29}$$

Since the elements of $|d|_\text{v} - \rho$ are nonpositive, $\dot{V}_2 \le 0$. Therefore, $x^{(2)}$ trajectories, which are on the sliding surface at $t = t_0$, will remain there for all $t > 0$. ∎

3.4 | Bounding the control signals

In this section, we provide a method, inspired by the work of Corradini et al,[59] to make sure that $|v_i| \le M_i$, where v_i refers to the ith element of the control signal v, and M_i is a positive scalar, $i = 1, 2, \ldots, \ell$, which is a predefined soft saturation limit. This ensures that $v_s = v$, which is an assumption used in the previous section. Note that the values of M_i are calculated using the information about actuator constraints and the control matrix. The actuator constraints are $u(t) \in \Omega_u = \{[u_1, ..., u_m]^T : u_{\min_i} \le u_i \le u_{\max_i}, i = 1, ..., m\}$. Using Ω_u, the set Ω_v, defining all realizable values of the control input v, can be obtained as $\Omega_v = \{v : v = Bu, u \in \Omega_u, B^\dagger v \in \Omega_u\}$, where $(.)^\dagger$ refers to the pseudo inverse of a nonsquare matrix. Furthermore, there exist M_i, $i = 1, ..., r$, such that $\hat{\Omega}_v \equiv \{v : v_i \in [-M_i, M_i], i = 1, ..., r\} \subset \Omega_v$. The set $\hat{\Omega}_v$ can be used to define the constraints which are enforced using a soft saturation function.[40]

We have observed in our simulation studies that the controller is robust for a range of cases where the assumption in Section 3.3 is violated. However, to have formal stability guarantees, we present sufficient conditions in this section that can be used to ensure that $v_s = v$. Later in the simulations section, we show that these conditions are indeed sufficient, not necessary, and even when they are violated good closed-loop performance is maintained.

Lemma 2. *The control signals v_i, $i = 1, 2, ..., \ell$, are bounded by M_i, $i = 1, 2, ..., \ell$, that is, $|v_i(t)| \leq M_i$ for all t if the inequality*

$$\left| -\sum_{\omega=1}^{n-\ell}\sum_{j=1}^{n-\ell} a_{2_{i,\omega}} \phi_{\omega,j}(t) x_j^{(1)}(0) - \int_0^t \left(\sum_{\omega=1}^{n-\ell}\sum_{j=1}^{n-\ell} a_{2_{i,\omega}} \phi_{\omega j}(t-\eta) \left[\sum_{k=n-\ell+1}^{n} a_{1_{j,k}} \left(x_{k-n+\ell}^{(2)}(0) e^{-\bar{\lambda}\eta} + r_{k-n+\ell}(\eta) \frac{2}{\pi} \tan^{-1}(\bar{\lambda}\eta) \right) \right] \right) d\eta \right.$$
$$\left. - \sum_{j=n-\ell+1}^{n} a_{2_{i,j}} \left(x_{j-n+\ell}^{(2)}(0) e^{-\bar{\lambda}t} + \frac{2}{\pi} r_{j-n+\ell}(t) \tan^{-1}(\bar{\lambda}t) \right) - \bar{\lambda} x_{n-\ell+i}(0) e^{-\bar{\lambda}t} + \frac{2}{\pi} \dot{r}_i(t) \tan^{-1}(\bar{\lambda}t) + \frac{2}{\pi} r_i(t) \frac{\bar{\lambda}}{1+\bar{\lambda}^2 t^2} \right| \leq M_i - \rho_i, \quad (30)$$

where $i = 1, ..., \ell$, is satisfied for all $t \geq 0$, where ρ is defined in Theorem 2, and $\phi_{i,j}(t)$ is the (i,j)th element of the state transition matrix $\Phi(t, t_0)$ in (22), with $t_0 = 0$.

Proof. See Appendix A. ∎

Remark 4. For (30) to be mathematically meaningful, its right-hand side, $M_i - \rho_i$, must be positive. It is shown in Tohidi et al.[40] that this is indeed the case.

The adjustable parameters in (30) are the initial values of the states $x(0) = [x^{(1)^T}(0), x^{(2)^T}(0)]^T$ and the scalar design parameter $\bar{\lambda}$. Assuming that the reference, $r(t)$, input vector and its rate of change are bounded, all of the terms in (30) are either bounded or converge to zero. Since $A_{1,1}$ is stable, the elements of state transition matrix, $\phi_{i,j}(t)$, converge to zero exponentially fast (see (22)). Specifically for the investigated flight control problem, the state transition matrix of $x^{(1)}$ dynamics (see (1)), where $x^{(1)} = [\alpha, \beta]^T$ and α and β are the angle of attack and the sideslip angle, respectively, consists of sums of decaying exponentials due to distinct eigenvalues. In this case, calculating the feasible values of the adjustable parameters becomes easier since the inequality (30) takes a simpler form, which is explained in the following corollary.

Corollary 1. *If the elements of the state transition matrix are formed as sums of exponential functions (which is the case in several flight control problems), that is, $\phi_{i,j}(t) = \sum_{\kappa=1}^{\bar{n}} c_{i,j_\kappa} e^{-h_{i,j_\kappa} t}$ with $h_{i,j_\kappa} > 0$ and $\bar{n}$ a positive integer, then the control signals v_i, $i = 1, ..., \ell$ are bounded by M_i, $i = 1, \ldots, \ell$, i.e. $|v_i| \leq M_i$ if the inequality*

$$W_i \equiv \left| -\sum_{\omega=1}^{n-\ell}\sum_{j=1}^{n-\ell}\sum_{\kappa=1}^{\bar{n}} a_{2_{i,\omega}} c_{\omega j_\kappa} e^{-h_{\omega j_\kappa} t} x_j^{(1)}(0) - \sum_{\omega=1}^{n-\ell}\sum_{j=1}^{n-\ell}\sum_{\kappa=1}^{\bar{n}}\sum_{k=n-\ell+1}^{n} a_{2_{i,\omega}} c_{\omega j_\kappa} a_{1_{j,k}} x_{k-n+\ell}^{(2)}(0) q_{\omega j_\kappa}(t) \right.$$
$$- \sum_{j=n-\ell+1}^{n} a_{2_{i,j}} \left(x_i^{(2)}(0) e^{-\bar{\lambda}t} + \frac{2}{\pi} r_i(t) \tan^{-1}(\bar{\lambda}t) \right) - \bar{\lambda} x_{n-\ell+i}(0) e^{-\bar{\lambda}t} + \frac{2}{\pi} \dot{r}_i(t) \tan^{-1}(\bar{\lambda}t) + \frac{2}{\pi} r_i(t) \frac{\bar{\lambda}}{1+\bar{\lambda}^2 t^2}$$
$$\left. + \int_0^t \sum_{\omega=1}^{n-\ell}\sum_{j=1}^{n-\ell}\sum_{\kappa=1}^{\bar{n}}\sum_{k=n-\ell+1}^{n} - a_{2_{i,\omega}} c_{\omega j_\kappa} e^{-h_{\omega j_\kappa}(t-\eta)} a_{1_{j,k}} r_{k-n+\ell}(\eta) \frac{2}{\pi} \tan^{-1}(\bar{\lambda}\eta) d\eta \right| \leq M_i - \rho_i, \quad i = 1, ..., \ell, \quad (31)$$

where

$$q_{\omega j_\kappa}(t) \equiv \begin{cases} t e^{-h_{\omega j_\kappa} t}, & \bar{\lambda} = h_{\omega j_\kappa}, \\ \frac{e^{-\bar{\lambda}t} - e^{-h_{\omega j_\kappa} t}}{h_{\omega j_\kappa} - \bar{\lambda}}, & \bar{\lambda} \neq h_{\omega j_\kappa}, \end{cases} \quad (32)$$

is satisfied for all $t \geq 0$.

Proof. See Appendix A.1. ∎

Remark 5. Given the upper and lower bounds of the reference signals and their derivatives, such that $r_i(t) \in [r_i^-, r_i^+]$ and $\dot{r}_i(t) \in [\dot{r}_i^-, \dot{r}_i^+]$, $r_i^- = -r_i^+$, $\dot{r}_i^- = -\dot{r}_i^+$, one way to check the inequality (31) is by using the triangle inequality and finding an upper bound for W_i as $\sum_{\omega=1}^{n-\ell}\sum_{j=1}^{n-\ell}\sum_{\kappa=1}^{\bar{n}} |a_{2_{i,\omega}} c_{\omega j_\kappa} x_j^{(1)}(0)| + \sum_{\omega=1}^{n-\ell}\sum_{j=1}^{n-\ell}\sum_{\kappa=1}^{\bar{n}}\sum_{k=n-\ell+1}^{n} |a_{2_{i,\omega}} c_{\omega j_\kappa} a_{1_{j,k}} x_{k-n+\ell}^{(2)}(0) \bar{q}_{\omega j_\kappa}| + \sum_{j=n-\ell+1}^{n} |a_{2_{i,j}} (x_i^{(2)}(0))| + \sum_{j=n-\ell+1}^{n} |a_{2_{i,j}} r_i^+| + |\bar{\lambda} x_{n-\ell+i}(0)| + |\dot{r}_i^+| + |\frac{2}{\pi} r_i^+ \bar{\lambda}| + \sum_{\omega=1}^{n-\ell}\sum_{j=1}^{n-\ell}\sum_{\kappa=1}^{\bar{n}}\sum_{k=n-\ell+1}^{n} |a_{2_{i,\omega}} c_{\omega j_\kappa} a_{1_{j,k}} \frac{r_{k-n+\ell}^+}{h_{\omega j_\kappa}}| \leq M_i - \rho_i$, where $\bar{q}_{\omega j_\kappa} = \max\{e^{-1} h_{\omega j_\kappa}^{-1}, \frac{2}{|h_{\omega j_\kappa} - \bar{\lambda}|}\}$. This inequality can be simplified as $W_{i,1} + \bar{\lambda} W_{i,2} \leq 0$, where $W_{i,1} = \sum_{\omega=1}^{n-\ell}\sum_{j=1}^{n-\ell}\sum_{\kappa=1}^{\bar{n}} |a_{2_{i,\omega}} c_{\omega j_\kappa} x_j^{(1)}(0)| + \sum_{\omega=1}^{n-\ell}\sum_{j=1}^{n-\ell}\sum_{\kappa=1}^{\bar{n}}\sum_{k=n-\ell+1}^{n} |a_{2_{i,\omega}} c_{\omega j_\kappa} a_{1_{j,k}} x_{k-n+\ell}^{(2)}(0) q_{\omega j_\kappa}(t)| + \sum_{j=n-\ell+1}^{n} |a_{2_{i,j}} (x_i^{(2)}(0))|$

$+\sum_{j=n-\ell+1}^{n}|a_{2_{i,j}}r_i^+| + |\dot{r}_i^+| + \sum_{\omega=1}^{n-\ell}\sum_{j=1}^{n-\ell}\sum_{\kappa=1}^{\bar{n}}\sum_{k=n-\ell+1}^{n}|a_{2_{i,\omega}}c_{\omega j_\kappa}a_{1_{j,k}}\frac{r^+_{k-n+\ell}}{h_{\omega j_\kappa}}| - M_i + \rho_i$ and $W_{i,2} = |x_{n-\ell+i}(0)| + |\frac{2}{\pi}r_i^+|$. Note that $W_{i,1}$ and $W_{i,2}$ are functions of $x^{(1)}(0)$, $x^{(2)}(0)$ and r_i^+, and remain constant along the closed-loop trajectory. Since $W_{i,2}$ is positive, a value of $\bar{\lambda} > 0$ satisfying $W_{i,1} + \bar{\lambda}W_{i,2} \le 0$ can always be found if $W_{i,1} < 0$, which can be realized by putting suitable bounds on the elements of $x^{(1)}(0)$, $x^{(2)}(0)$, and r. This procedure is conservative due to the nature of the triangular inequality. On the other hand, if the reference signal trajectories are known, one can check the inequality (31) numerically. We demonstrate the application of the latter approach in the simulation results sections.

For a constant reference input vector r, the inequality (31) can be simplified further. This is described in the following corollary.

Corollary 2. *If, in addition to the conditions given in Corollary 1, the reference signals are constant, that is, $r_i(t) = R_i$, $i = 1, ..., \ell$, then the control signals v_i, $i = 1, ..., \ell$ are bounded by M_i, $i = 1, ..., \ell$, i.e. $|v_i| \le M_i$, if the inequality*

$$\begin{aligned}\hat{W}_i \equiv \Bigg| &-\sum_{\omega=1}^{n-\ell}\sum_{j=1}^{n-\ell}\sum_{\kappa=1}^{\bar{n}} a_{2_{i,\omega}}c_{\omega j_\kappa}e^{-h_{\omega j_\kappa}t}x_j^{(1)}(0) - \sum_{\omega=1}^{n-\ell}\sum_{j=1}^{n-\ell}\sum_{\kappa=1}^{\bar{n}}\sum_{k=n-\ell+1}^{n} a_{2_{i,\omega}}c_{\omega j_\kappa}a_{1_{j,k}}x^{(2)}_{k-n+\ell}(0)q_{\omega j_\kappa}(t)\\ &- \sum_{j=n-\ell+1}^{n} a_{2_{i,j}}\left(x_i^{(2)}(0)e^{-\bar{\lambda}t} + \frac{2}{\pi}R_i\tan^{-1}(\bar{\lambda}t)\right) - \bar{\lambda}x_{n-\ell+i}(0)e^{-\bar{\lambda}t} + \frac{2}{\pi}R_i\frac{\bar{\lambda}}{1+\bar{\lambda}^2t^2}\Bigg|\\ &+ \sum_{\omega=1}^{n-\ell}\sum_{j=1}^{n-\ell}\sum_{\kappa=1}^{\bar{n}}\left|\sum_{k=n-\ell+1}^{n} - a_{2_{i,\omega}}c_{\omega j_\kappa}a_{1_{j,k}}R_{k-n+\ell}\right|\frac{1-e^{-h_{\omega j_\kappa}t}}{h_{\omega j_\kappa}} \le M_i - \rho_i, \quad i = 1, ..., \ell,\end{aligned} \tag{33}$$

where $q_{\omega j_\kappa}(t)$ is defined in (32), is satisfied for all $t \ge 0$.

Proof. The proof is similar to that of Corollary 1. ∎

Remark 6. The left-hand side of the inequality (33) can be written as $|k_1e^{-\bar{\lambda}t} + k_2e^{-h_{\omega j_\kappa}t} + k_3\frac{\bar{\lambda}}{1+\bar{\lambda}^2t^2} + k_4\frac{2}{\pi}\tan^{-1}(\bar{\lambda}t) + k_5|$, where k_i, $i = 1, 2, ..., 5$ are the appropriate constant coefficients. Since all of the terms are monotonic functions, it is enough to check (33) at $t = 0$, $t = \infty$ and at the extremum points in between, if any. Extremum points can be found by taking the derivative and equating it to zero and finding the roots numerically.

4 | SIMULATION RESULTS

The ADMIRE, which represents the dynamics of an over-actuated aircraft model, is used to demonstrate the effectiveness of the proposed controller. The linearized ADMIRE model[29] is given as

$$\begin{aligned}\dot{x} &= Ax + B_uu = Ax + B_vv_s,\\ v_s &= Bu, \quad B_u = B_vB, \quad B_v = [0_{3\times2}\ I_{3\times3}]^T,\end{aligned} \tag{34}$$

where $x = [\alpha\ \beta\ p\ q\ r]^T$ with α, β, p, q, and r denote the angle of attack, sideslip angle, roll rate, pitch rate, and yaw rate, respectively. The vector $u = [u_c\ u_{re}\ u_{le}\ u_r]^T$ represents the control surface deflections of canard wings, right and left elevons and the rudder. The position limits of the control surfaces are given as $u_c \in [-55, 25] \times \frac{\pi}{180}$ rad, $u_{re}, u_{le}, u_r \in [-30, 30] \times \frac{\pi}{180}$ rad. The actuators have first-order dynamics with a time constant of 0.05 s. The state and control matrices are provided by Härkegård et al.[29] To represent actuator loss of effectiveness and disturbance, a diagonal matrix Λ and a vector d_u, respectively, are introduced in the model (34) as

$$\begin{aligned}\dot{x} &= Ax + B_u\Lambda u + B_ud_u = Ax + B_vv_s + B_v\bar{d},\\ v_s &= B\Lambda u + \bar{d}, \quad \bar{d} = Bd_u, \quad B_u = B_vB, \quad B_v = [0_{3\times2}\ I_{3\times3}]^T.\end{aligned} \tag{35}$$

A sinusoidal function with amplitude of 0.1 and frequency of 1 rad/s is considered as the disturbance $\bar{d}$ in the simulation. Saturation limits are calculated as $M_1 = 1.4$, $M_2 = 1.4$ and $M_3 = 0.3$. Furthermore, the maximum and minimum range of the elements of θ_v for the projection algorithm are taken as $\theta_{v_{1,1}} \in [-0.0129, 0.0129]$, $\theta_{v_{1,2}} \in [0.0307, 0.5225]$,

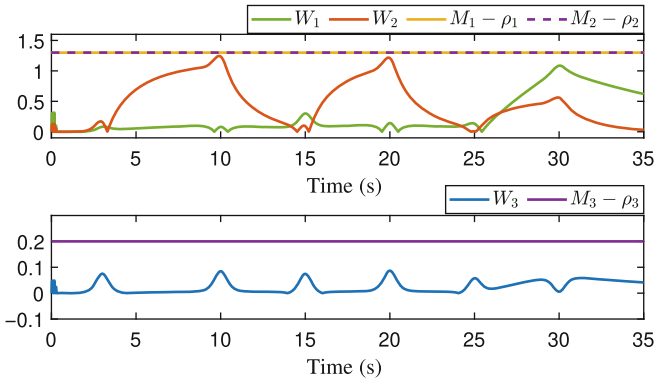

FIGURE 2 Validation of the inequality (31)

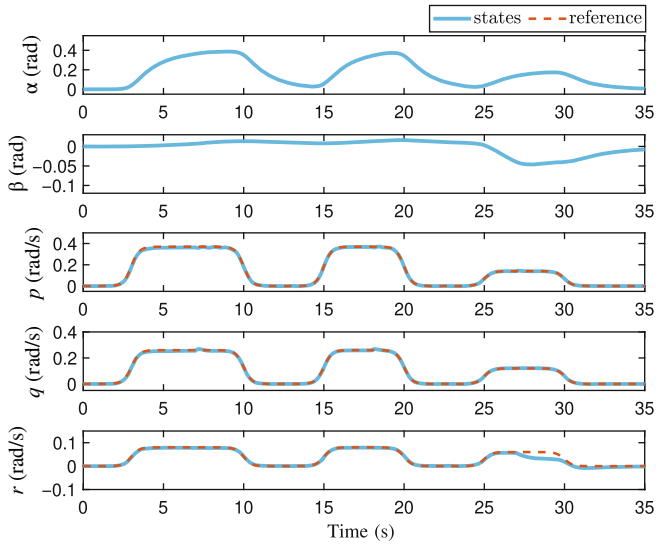

FIGURE 3 Time evolution of the aircraft states and the references, in the presence of actuator uncertainty. At $t = 7$ s, $t = 18$ s and $t = 27$ s, 15%, 30%, and 35%–70% losses of effectiveness are introduced, respectively.

$\theta_{v_{1,3}} \in [-0.1357, 0.1371]$, $\theta_{v_{1,4}} \in [-0.212, 0]$, $\theta_{v_{2,1}} \in [-0.3149, -0.1113]$, $\theta_{v_{2,2}} \in [-0.217, -0.1416]$, $\theta_{v_{2,3}} \in [-0.0241, 0.2363]$, $\theta_{v_{2,4}} \in [-0.4162, -0.01]$, $\theta_{v_{3,1}} \in [0.1587, 0.1977]$, $\theta_{v_{3,2}} \in [0.0673, 0.0675]$, $\theta_{v_{3,3}} \in [-0.001, 0.001]$, and $\theta_{v_{3,4}} \in [-1.2755, -0.7641]$ (see Tohidi et al.[40] for how these values can be calculated). The proposed sliding mode controller is implemented using $\bar{\lambda} = 3$ (see (26)). To avoid chattering, the boundary layer approach[64] is used. The actuator loss of effectiveness is modeled as

$$\Lambda(t) = \begin{cases} diag(1,1,1,1) & for \;\; t \leq 7, \\ \text{diag}(0.85, 0.85, 0.85, 0.85) & \text{for} \;\; 7 < t \leq 18, \\ \text{diag}(0.7, 0.7, 0.7, 0.7) & \text{for} \;\; 18 < t \leq 27, \\ \text{diag}(0.65, 0.6, 0.65, 0.3) & \text{for} \;\; 27 < t. \end{cases}$$

Since $A_{1,1}$ in the ADMIRE model has distinct real eigenvalues, we can use Corollary 1, which requires (31) to be satisfied. The reference signals are chosen as

$$r_i(t) = \gamma_i \left(\frac{1}{1+e^{-4(t-3)}} - \frac{1}{1+e^{-4(t-10)}} + \frac{1}{1+e^{-4(t-15)}} - \frac{1}{1+e^{-4(t-20)}} \right) + \hat{\gamma}_i \left(\frac{1}{1+e^{-4(t-25)}} - \frac{1}{1+e^{-4(t-30)}} \right), \quad i = 1, 2, 3, \tag{36}$$

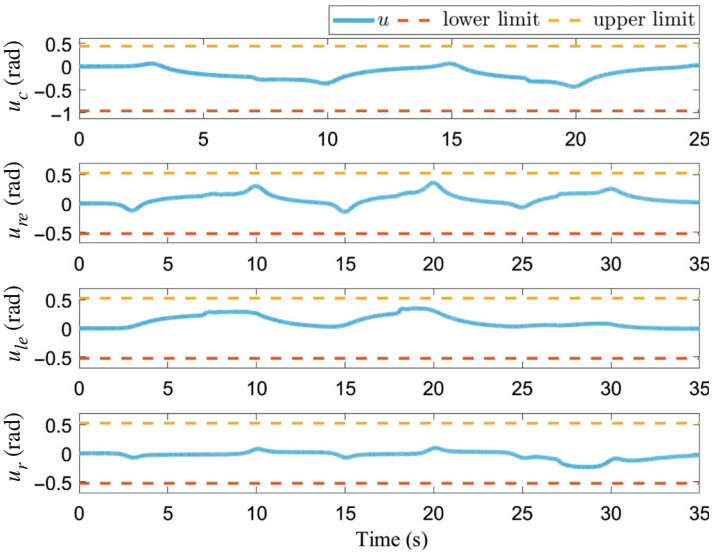

FIGURE 4 Time evolution of the control surfaces

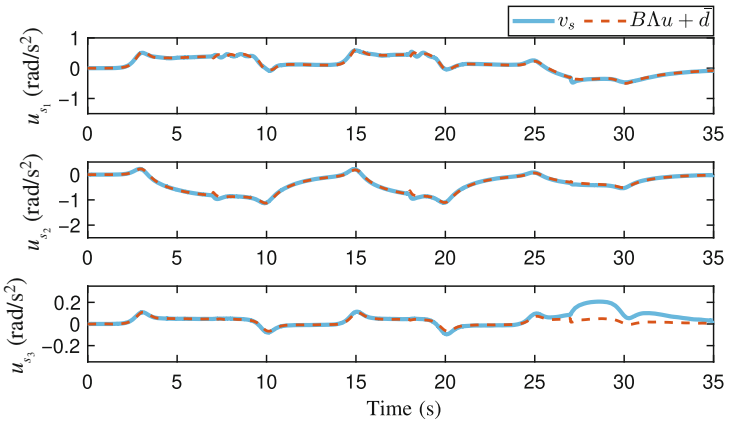

FIGURE 5 Control allocation performance

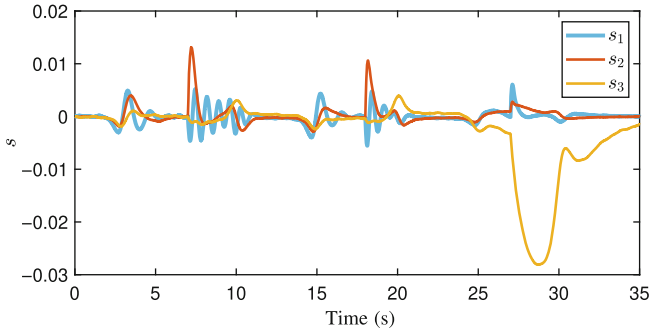

FIGURE 6 The evolution of the sliding surfaces

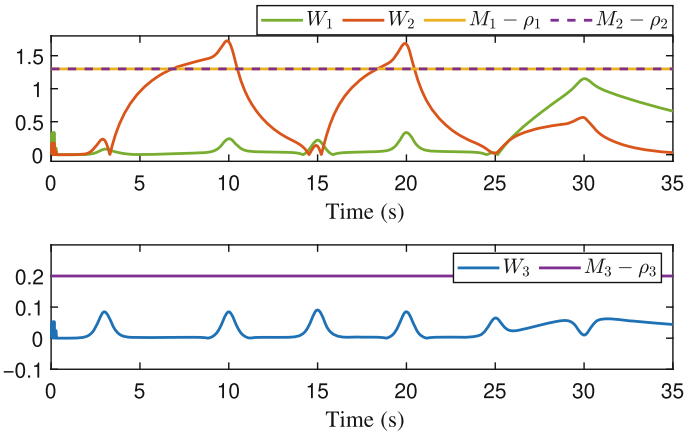

FIGURE 7 The case when the inequality (31) is not satisfied

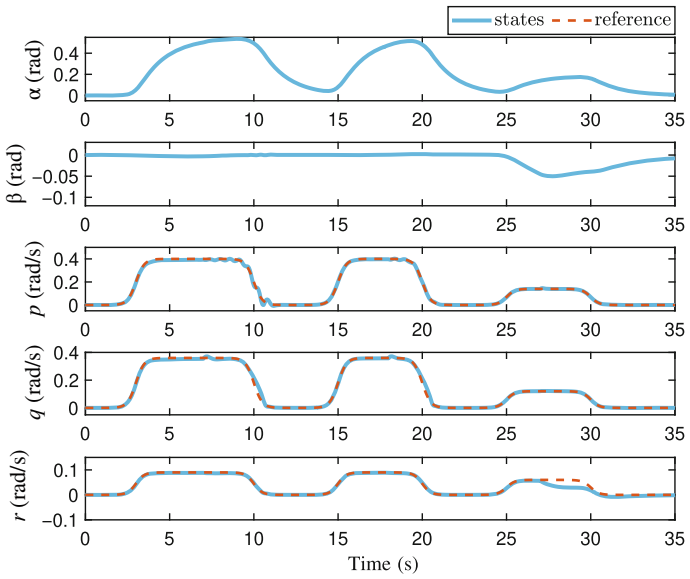

FIGURE 8 Time evolution of the states when (31) is violated

where $\gamma_1 = 0.37$, $\gamma_2 = 0.26$, $\gamma_3 = 0.08$, $\hat{\gamma}_1 = 0.14$, $\hat{\gamma}_2 = 0.12$ and $\hat{\gamma}_3 = 0.06$. It is seen in Figure 2 that the inequality (31) is satisfied for $i = 1, 2, 3$.

Figure 3 illustrates the time evolution of the states when 15% actuator loss of effectiveness occurs at $t = 7$ s, 30% at $t = 18$ s and 35%–70% at $t = 27$ s. The states remain bounded and p, q, and r follow the reference signals. Figure 4 demonstrates the control surface deflections together with the saturation limits. The actuators stay within their limits. The performance of the control allocation is depicted in Figure 5. It shows that the control allocation determines the actuator input vector u in such a way that $B\Lambda u + \bar{d}$ follows the control signal v_s. Figure 6 shows the sliding surface trajectories, which tend to grow at the times of uncertainty injections but converge to a neighborhood of zero afterwards, without any chattering effect.

In order to show the robustness of the proposed method, we examine the case where the inequality (31) is violated. The violation is realized by setting the parameters γ_is and $\hat{\gamma}_i$s in (36) to $\gamma_1 = 0.4$, $\gamma_2 = 0.35$, $\gamma_3 = 0.09$, $\hat{\gamma}_1 = 0.14$, $\hat{\gamma}_2 = 0.12$ and $\hat{\gamma}_3 = 0.06$. It is seen in Figure 7 that the inequality (31) is violated by W_2. Figures 8–11 illustrate that even though (31) is not satisfied, the system remains stable, while tracking its references. Thus the controller is able to provide reasonable performance even when the inequality (31), which is a sufficient condition, is violated; the investigation of additional sufficient conditions, motivated by our simulation-based observations of the method's robustness, is left as a topic for continuing research.

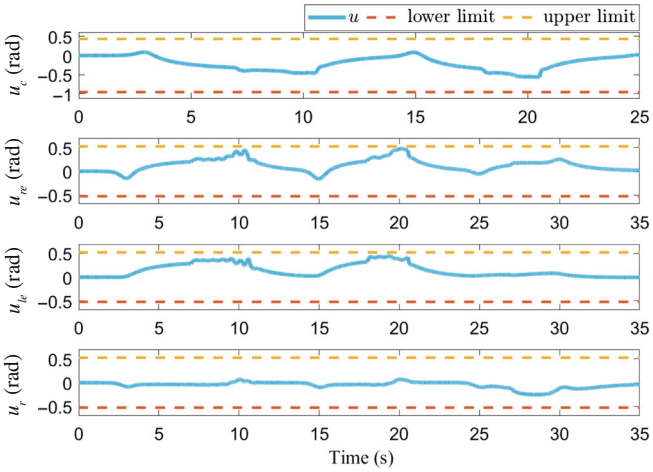

FIGURE 9 Time evolution of the control surfaces when (31) is violated

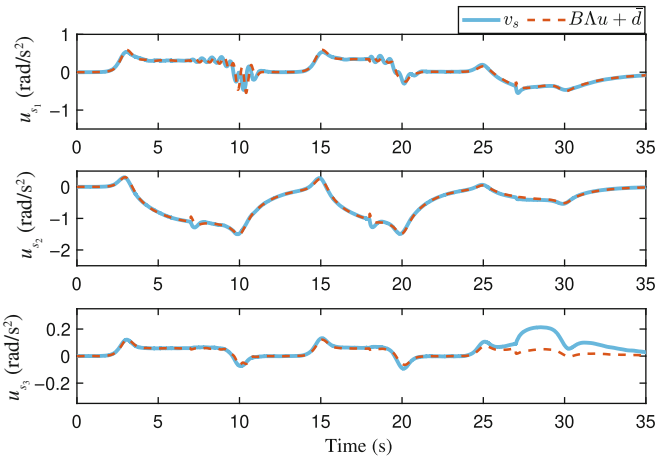

FIGURE 10 Control allocation performance when (31) is violated. Control allocation signal v_s does not saturate, and therefore $v_s = v$ (see Figure 1).

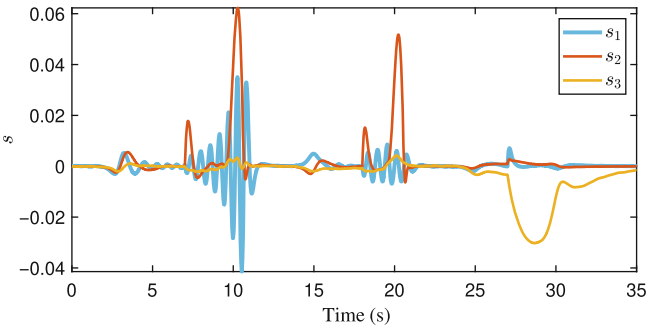

FIGURE 11 The evolution of the sliding surfaces when (31) is violated

5 | SUMMARY

In this paper, a sliding mode controller with a time-varying sliding surface is proposed to complement an adaptive control allocator for uncertain over-actuated systems with actuator saturation. Stability of the overall closed-loop system is shown using Lyapunov arguments. Simulation results with the ADMIRE model show the effectiveness of the proposed method.

ORCID

Seyed Shahabaldin Tohidi https://orcid.org/0000-0002-4566-667X
Yildiray Yildiz https://orcid.org/0000-0001-6270-5354
Ilya Kolmanovsky https://orcid.org/0000-0002-7225-4160

REFERENCES

1. Yildiz Y, Kolmanovsky I. Stability properties and cross-coupling performance of the control allocation scheme CAPIO. *J Guid Control Dyn*. 2011;34(4):1190-1196.
2. Ducard GJ. *Fault-Tolerant Flight Control and Guidance Systems: Practical Methods for Small Unmanned Aerial Vehicles*. Springer Science & Business Media; 2009.
3. Bodson M. Evaluation of optimization methods for control allocation. *J Guid Control Dyn*. 2002;25(4):703-711.
4. Liao F, Lum K-Y, Wang JL, Benosman M. Adaptive control allocation for non-linear systems with internal dynamics. *IET Control Theory Appl*. 2010;4(6):909-922.
5. Shen Q, Wang D, Zhu S, Poh EK. Inertia-free fault-tolerant spacecraft attitude tracking using control allocation. *Automatica*. 2015;62:114-121.
6. Yildiz Y, Kolmanovsky I. Implementation of CAPIO for composite adaptive control of cross-coupled unstable aircraft. *Infotech Aerosp*. 2011:1460.
7. Acosta DM, Yildiz Y, Craun RW, et al. Piloted evaluation of a control allocation technique to recover from pilot-induced oscillations. *J Aircr*. 2014;52(1):130-140.
8. Shen Q, Wang D, Zhu S, Poh EK. Robust control allocation for spacecraft attitude tracking under actuator faults. *IEEE Trans Control Syst Technol*. 2017;25(3):1068-1075.
9. Sadeghzadeh I, Chamseddine A, Zhang Y, Theilliol D. Control allocation and re-allocation for a modified quadrotor helicopter against actuator faults. *IFAC Proc Vol*. 2012;45(20):247-252.
10. Tohidi SS, Yildiz Y, Kolmanovsky I. Pilot induced oscillation mitigation for unmanned aircraft systems: an adaptive control allocation approach. Proceedings of the IEEE Conference on Control Technology and Applications; 2018:343-348.
11. Podder TK, Sarkar N. Fault-tolerant control of an autonomous underwater vehicle under thruster redundancy. *Robot Auton Syst*. 2001;34(1):39-52.
12. Gierusz W, Tomera M. Logic thrust allocation applied to multivariable control of the training ship. *Control Eng Pract*. 2006;14(5):511-524.
13. Johansen TA, Fuglseth TP, Tøndel P, Fossen TI. Optimal constrained control allocation in marine surface vessels with rudders. *Control Eng Pract*. 2008;16(4):457-464.
14. Chen M, Ge SS, How BVE, Choo YS. Robust adaptive position mooring control for marine vessels. *IEEE Trans Control Syst Technol*. 2013;21(2):395-409.
15. Sørensen AJ. A survey of dynamic positioning control systems. *Annu Rev Control*. 2011;35(1):123-136.
16. Corradini ML, Cristofaro A. A nonlinear fault-tolerant thruster allocation architecture for underwater remotely operated vehicles. *IFAC-PapersOnLine*. 2016;49(23):285-290.
17. Tjønnås J, Johansen TA. Stabilization of automotive vehicles using active steering and adaptive brake control allocation. *IEEE Trans Control Syst Technol*. 2010;18(3):545-558.
18. Temiz O, Cakmakci M, Yildiz Y. A fault tolerant vehicle stability control using adaptive control allocation. Proceedings of the Dynamic Systems and Control Conference; 2018.
19. Temiz O, Cakmakci M, Yildiz Y. A fault tolerant integrated vehicle stability control using adaptive control allocation. arXiv preprint arXiv:2008.05697; 2020.
20. Tohidi SS, Khaki Sedigh A. Adaptive fault tolerance in automotive vehicle using control allocation based on the pseudo inverse along the null space for yaw stabilization. Proceedings of the 3rd International Conference on Control, Instrumentation, and Automation; 2013:174-179.
21. Taghirad HD, Bedoustani YB. An analytic-iterative redundancy resolution scheme for cable-driven redundant parallel manipulators. *IEEE Trans Robot*. 2011;27(6):1137-1143.
22. Bouarfa A, Bodson M, Fadel M. A fast active-balancing method for the 3-phase multilevel flying capacitor inverter derived from control allocation theory. *IFAC-PapersOnLine*. 2017;50(1):2113-2118.
23. Raoufat ME, Tomsovic K, Djouadi SM. Dynamic control allocation for damping of inter-area oscillations. *IEEE Trans Power Syst*. 2017;32(6):4894-4903.
24. Durham WC. Constrained control allocation. *J Guid Control Dyn*. 1993;16(4):717-725.
25. Durham W, Bordignon KA, Beck R. *Aircraft Control Allocation*. Springer Science & Business Media; 2017.
26. Alwi H, Edwards C. Fault tolerant control using sliding modes with on-line control allocation. *Automatica*. 2008;44(7):1859-1866.

27. Tohidi SS, Khaki Sedigh A, Buzorgnia D. Fault tolerant control design using adaptive control allocation based on the pseudo inverse along the null space. *Int J Robust Nonlinear Control*. 2016;26(16):3541-3557.
28. Petersen JA, Bodson M. Constrained quadratic programming techniques for control allocation. *IEEE Trans Control Syst Technol*. 2006;14(1):91-98.
29. Härkegård O, Glad ST. Resolving actuator redundancy-optimal control vs. Control allocation. *Automatica*. 2005;41(1):137-144.
30. Casavola A, Garone E. Fault-tolerant adaptive control allocation schemes for overactuated systems. *Int J Robust Nonlinear Control*. 2010;20(17):1958-1980.
31. Härkegård O. Efficient active set algorithms for solving constrained least squares problems in aircraft control allocation. Proceedings of the IEEE Conference on Decision and Control; 2002:1295-1300.
32. Yildiz Y, Kolmanovsky IV. A control allocation technique to recover from pilot-induced oscillations (CAPIO) due to actuator rate limiting. Proceedings of the American Control Conference; 2010:516-523.
33. Yildiz Y, Kolmanovsky IV, Acosta D. A control allocation system for automatic detection and compensation of phase shift due to actuator rate limiting. Proceedings of the American Control Conference; 2011:444-449.
34. Zaccarian L. Dynamic allocation for input redundant control systems. *Automatica*. 2009;45(6):1431-1438.
35. Tjønnås J, Johansen TA. Adaptive control allocation. *Automatica*. 2008;44(11):2754-2765.
36. Falconi GP, Holzapfel F. Adaptive fault tolerant control allocation for a hexacopter system. Proceedings of the American Control Conference (ACC); 2016:6760-6766.
37. Tohidi SS, Yildiz Y, Kolmanovsky I. Fault tolerant control for over-actuated systems: an adaptive correction approach. Proceedings of the American Control Conference; 2016:2530-2535.
38. Tohidi SS, Yildiz Y, Kolmanovsky I. Adaptive control allocation for over-actuated systems with actuator saturation. *IFAC-PapersOnLine*. 2017;50(1):5492-5497.
39. Galeani S, Sassano M. Data-driven dynamic control allocation for uncertain redundant plants. Proceedings of the IEEE Conference on Decision and Control; 2018:5494-5499.
40. Tohidi SS, Yildiz Y, Kolmanovsky I. Adaptive control allocation for constrained systems. *Automatica*. 2020;121:109161.
41. Johansen TA, Fossen TI. Control allocation—A survey. *Automatica*. 2013;49(5):1087-1103.
42. Tarbouriech S, Garcia G, Silva JM Jr, Queinnec I. *Stability and Stabilization of Linear Systems with Saturating Actuators*. Springer Science & Business Media; 2011.
43. Buffington JM, Enns DF. Lyapunov stability analysis of daisy chain control allocation. *J Guid Control Dyn*. 1996;19(6):1226-1230.
44. Molnar L, Omerdic E, Toal D. Guidance, navigation and control system for the Tethra unmanned underwater vehicle. *Int J Control*. 2007;80(7):1050-1076.
45. Safa A, Baradarannia M, Kharrati H, Khanmohammadi S. Robust attitude tracking control for a rigid spacecraft under input delays and actuator errors. *Int J Control*. 2019;92(5):1183-1195.
46. Naskar AK, Patra S, Sen S. New control allocation algorithms in fixed point framework for overactuated systems with actuator saturation. *Int J Control*. 2017;90(2):348-356.
47. Naderi M, Sedigh AK, Johansen TA. Guaranteed feasible control allocation using model predictive control. *Control Theory Technol*. 2019;17(3):252-264.
48. Tohidi SS, Yildiz Y. Handling actuator magnitude and rate saturation in uncertain over-actuated systems: a modified projection algorithm approach. *Int J Control*. 2020;95(3):790-803.
49. Rios H, Kamal S, Fridman LM, Zolghadri A. Fault tolerant control allocation via continuous integral sliding-modes: a HOSM-observer approach. *Automatica*. 2015;51:318-325.
50. Chen L, Edwards C, Alwi H, Sato M. Flight evaluation of a sliding mode online control allocation scheme for fault tolerant control. *Automatica*. 2020;114:108829.
51. Steinberger M, Castillo I, Horn M, Fridman L. Robust output tracking of constrained perturbed linear systems via model predictive sliding mode control. *Int J Robust Nonlinear Control*. 2020;30(3):1258-1274.
52. Incremona GP, Ferrara A, Magni L. Hierarchical model predictive/sliding mode control of nonlinear constrained uncertain systems. *IFAC-PapersOnLine*. 2015;48(23):102-109.
53. Rubagotti M, Raimondo DM, Ferrara A, Magni L. Robust model predictive control with integral sliding mode in continuous-time sampled-data nonlinear systems. *IEEE Trans Automat Contr*. 2010;56(3):556-570.
54. Raimondo DM, Rubagotti M, Jones CN, Magni L, Ferrara A, Morari M. Multirate sliding mode disturbance compensation for model predictive control. *Int J Robust Nonlinear Control*. 2015;25(16):2984-3003.
55. Golkani MA, Seeber R, Reichhartinger M, Horn M. Lyapunov-based saturated continuous twisting algorithm. *Int J Robust Nonlinear Control*. 2021;31(9):3513-3527.
56. Ferrara A, Incremona GP, Regolin E. Optimization-based adaptive sliding mode control with application to vehicle dynamics control. *Int J Robust Nonlinear Control*. 2019;29(3):550-564.
57. Seeber R, Reichhartinger M. Conditioned super-twisting algorithm for systems with saturated control action. *Automatica*. 2020;116:108921.
58. Seeber R, Horn M. Guaranteeing disturbance rejection and control signal continuity for the saturated super-twisting algorithm. *IEEE Control Syst Lett*. 2019;3(3):715-720.
59. Corradini ML, Cristofaro A, Orlando G. Robust stabilization of multi input plants with saturating actuators. *IEEE Trans Automat Contr*. 2010;55(2):419-425.

60. Tohidi SS, Yildiz Y, Kolmanovsky I. Sliding mode control for over-actuated systems with adaptive control allocation and its applications to flight control. Proceedings of the 2021 IEEE Conference on Control Technology and Applications (CCTA); 2021:765-770.
61. Eugene L, Kevin W, Howe D. *Robust and Adaptive Control with Aerospace Applications*. Springer; 2013.
62. Stevens BL, Lewis FL, Johnson EN. *Aircraft Control and Simulation: Dynamics, Controls Design, and Autonomous Systems*. John Wiley & Sons; 2015.
63. Antsaklis PJ, Michel AN. *Linear Systems*. Springer Science & Business Media; 2006.
64. Slotine J-JE, Li W. *Applied Nonlinear Control*. Prentice Hall; 1991.
65. Utkin V, Shi J. Integral sliding mode in systems operating under uncertainty conditions. Proceedings of 35th IEEE Conference on Decision and Control; 1996:4591-4596.
66. Nechepurenko YM. Bounds for the matrix exponential based on the Lyapunov equation and limits of the Hausdorff set. *Comput Math Math Phys*. 2002;42(2):125-134.

How to cite this article: Tohidi SS, Yildiz Y, Kolmanovsky I. Time-varying sliding mode controller for over-actuated systems with constrained and uncertain actuators in flight control applications. *Int J Robust Nonlinear Control*. 2023;33(3):1720-1737. doi: 10.1002/rnc.6440

APPENDIX. PROOF OF LEMMA 2

Rewriting (26) using the matrices in (16), we have

$$\begin{bmatrix} v_1(t) \\ \vdots \\ v_\ell(t) \end{bmatrix} = -\begin{bmatrix} a_{2_{1,1}} & \cdots & a_{2_{1,(n-\ell)}} \\ \vdots & \ddots & \vdots \\ a_{2_{\ell,1}} & \cdots & a_{2_{\ell,(n-\ell)}} \end{bmatrix}\begin{bmatrix} x_1^{(1)}(t) \\ \vdots \\ x_{n-\ell}^{(1)}(t) \end{bmatrix} - \begin{bmatrix} a_{2_{1,(n-\ell+1)}} & \cdots & a_{2_{1,n}} \\ \vdots & \ddots & \vdots \\ a_{2_{\ell,(n-\ell+1)}} & \cdots & a_{2_{\ell,n}} \end{bmatrix}\begin{bmatrix} x_1^{(2)}(t) \\ \vdots \\ x_\ell^{(2)}(t) \end{bmatrix} - \bar{\lambda}e^{-\bar{\lambda}t}\begin{bmatrix} x_1^{(2)}(0) \\ \vdots \\ x_\ell^{(2)}(0) \end{bmatrix} + \frac{2}{\pi}\tan^{-1}(\bar{\lambda}t)\begin{bmatrix} \dot{r}_1(t) \\ \vdots \\ \dot{r}_\ell(t) \end{bmatrix}$$
$$+ \frac{2}{\pi}\frac{\bar{\lambda}}{1+\bar{\lambda}^2t^2}\begin{bmatrix} r_1(t) \\ \vdots \\ r_\ell(t) \end{bmatrix} - \begin{bmatrix} \bar{s}_1(t) & 0 & 0 & \cdots & 0 \\ 0 & \bar{s}_2(t) & 0 & \cdots & 0 \\ \vdots & \vdots & \ddots & \cdots & \vdots \\ 0 & \cdots & 0 & \bar{s}_{\ell-1}(t) & 0 \\ 0 & \cdots & 0 & 0 & \bar{s}_\ell(t) \end{bmatrix}\begin{bmatrix} \rho_1 \\ \vdots \\ \rho_\ell \end{bmatrix}, \tag{A1}$$

where $a_{2_{i,j}}$, $i = 1, \ldots, \ell, j = 1, \ldots, n-\ell$ are the elements of $A_{2,1}$, and $a_{2_{i,j}}$, $i = 1, ..., \ell, j = n-\ell+1, ..., n$ are the elements of $A_{2,2}$. Also, $x_i^{(2)}$, r_i, $\dot{r}_i$ and ρ_i, $i = 1, ..., \ell$ are the elements of the vectors $x^{(2)}$, r, $\dot{r}$, and ρ, respectively, and $\bar{s}_i$ are the ith diagonal element of $\text{sign}_{\text{v}}\left(s(x^{(2)}(t), x^{(2)}(0), t)\right)$. Thus,

$$v_i(t) = -\sum_{j=1}^{n-\ell} a_{2_{i,j}} x_j^{(1)}(t) - \sum_{j=n-\ell+1}^{n} a_{2_{i,j}} x_{j-n+\ell}^{(2)}(t) - \bar{\lambda}x_i^{(2)}(0)e^{-\bar{\lambda}t} + \frac{2}{\pi}\dot{r}_i(t)\tan^{-1}(\bar{\lambda}t) + \frac{2}{\pi}r_i(t)\frac{\bar{\lambda}}{1+\bar{\lambda}^2t^2} - \bar{s}_i(t)\rho_i. \tag{A2}$$

To ensure that $|v_i| \le M_i$ for $i = 1, \ldots, \ell$, the inequality

$$\left| -\sum_{j=1}^{n-\ell} a_{2_{i,j}} x_j^{(1)}(t) - \sum_{j=n-\ell+1}^{n} a_{2_{i,j}} x_{j-n+\ell}^{(2)}(t) - \bar{\lambda}x_i^{(2)}(0)e^{-\bar{\lambda}t} + \frac{2}{\pi}\dot{r}_i(t)\tan^{-1}(\bar{\lambda}t) + \frac{2}{\pi}r_i(t)\frac{\bar{\lambda}}{1+\bar{\lambda}^2t^2} - \bar{s}_i(t)\rho_i \right| \le M_i, \tag{A3}$$

should be satisfied for all $i = 1, ..., \ell$.

By considering the elements of $\Phi(t, t_0)$ as $\phi_{i,j}(t)$, $i = 1, ..., n-\ell, j = 1, ..., n-\ell$, with $t_0 = 0$, and substituting these in (23), we have

$$\begin{bmatrix} x_1^{(1)}(t) \\ \vdots \\ x_{n-\ell}^{(1)}(t) \end{bmatrix} = \begin{bmatrix} \phi_{1,1}(t) & \cdots & \phi_{1,(n-\ell)}(t) \\ \vdots & \cdots & \vdots \\ \phi_{(n-\ell),1}(t) & \cdots & \phi_{(n-\ell),(n-\ell)}(t) \end{bmatrix}\begin{bmatrix} x_1^{(1)}(0) \\ \vdots \\ x_{n-\ell}^{(1)}(0) \end{bmatrix} + \int_0^t \begin{bmatrix} \phi_{1,1}(t-\eta) & \cdots & \phi_{1,(n-\ell)}(t-\eta) \\ \vdots & \cdots & \vdots \\ \phi_{(n-\ell),1}(t-\eta) & \cdots & \phi_{(n-\ell),(n-\ell)}(t-\eta) \end{bmatrix}\begin{bmatrix} g_1(\eta) \\ \vdots \\ g_{n-\ell}(\eta) \end{bmatrix} d\eta. \tag{A4}$$

Remembering that $g(t) \equiv G_1 e^{-\bar{\lambda}(t-t_0)} + G_2(t)$, with $G_1 \equiv A_{1,2}x^{(2)}(t_0)$, and $G_2(t) \equiv \frac{2}{\pi}A_{1,2}r(t)\tan^{-1}(\bar{\lambda}(t-t_0))$, the elements of the vector $g(t)$ can be written as

$$\begin{bmatrix} g_1(t) \\ \vdots \\ g_{n-\ell}(t) \end{bmatrix} = \begin{bmatrix} a_{1_{1,(n-\ell+1)}} & \cdots & a_{1_{1,n}} \\ \vdots & \ddots & \vdots \\ a_{1_{(n-\ell),(n-\ell+1)}} & \cdots & a_{1_{(n-\ell),n}} \end{bmatrix} \begin{bmatrix} x_1^{(2)}(0) \\ \vdots \\ x_\ell^{(2)}(0) \end{bmatrix} e^{-\bar{\lambda}t} + \frac{2}{\pi}\tan^{-1}(\bar{\lambda}t) \begin{bmatrix} a_{1_{1,(n-\ell+1)}} & \cdots & a_{1_{1,n}} \\ \vdots & \ddots & \vdots \\ a_{1_{(n-\ell),(n-\ell+1)}} & \cdots & a_{1_{(n-\ell),n}} \end{bmatrix} \begin{bmatrix} r_1(t) \\ \vdots \\ r_\ell(t) \end{bmatrix}. \tag{A5}$$

Substituting (A5) into (A4), the ith element of the vector $x^{(1)}(t)$ can be written as

$$x_i^{(1)}(t) = \sum_{j=1}^{n-\ell} \phi_{i,j}(t)x_j^{(1)}(0) + \int_0^t \left(\sum_{j=1}^{n-\ell} \phi_{i,j}(t-\eta) \left[\sum_{k=n-\ell+1}^{n} a_{1_{j,k}} \left(x_{k-n+\ell}^{(2)}(0)e^{-\bar{\lambda}\eta} + r_{k-n+\ell}(\eta)\frac{2}{\pi}\tan^{-1}(\bar{\lambda}\eta) \right) \right] \right) d\eta, \quad i = 1, ..., n-\ell, \tag{A6}$$

where $a_{1_{j,k}}$ refer to the elements of A_1. Substituting (A6) and the elements of $x^{(2)}$ (see (19)) in (A3), we have

$$\begin{aligned} |v_i(t)| = \Bigg| & -\sum_{\omega=1}^{n-\ell}\sum_{j=1}^{n-\ell} a_{2_{i,\omega}}\phi_{\omega,j}(t)x_j^{(1)}(0) \\ & - \int_0^t \left(\sum_{\omega=1}^{n-\ell}\sum_{j=1}^{n-\ell} a_{2_{i,\omega}}\phi_{\omega,j}(t-\eta) \left[\sum_{k=n-\ell+1}^{n} a_{1_{j,k}} \left(x_{k-n+\ell}^{(2)}(0)e^{-\bar{\lambda}\eta} + r_{k-n+\ell}(\eta)\frac{2}{\pi}\tan^{-1}(\bar{\lambda}\eta) \right) \right] \right) d\eta \\ & - \sum_{j=n-\ell+1}^{n} a_{2_{i,j}} \left(x_{j-n+\ell}^{(2)}(0)e^{-\bar{\lambda}t} + \frac{2}{\pi}r_{j-n+\ell}(t)\tan^{-1}(\bar{\lambda}t) \right) \\ & - \bar{\lambda}x_{n-\ell+i}(0)e^{-\bar{\lambda}t} + \frac{2}{\pi}\dot{r}_i(t)\tan^{-1}(\bar{\lambda}t) + \frac{2}{\pi}r_i(t)\frac{\bar{\lambda}}{1+\bar{\lambda}^2t^2} - \bar{s}_i(x(t))\rho_i \Bigg| \leq M_i, \end{aligned} \tag{A7}$$

for $i = 1, ..., \ell$. Using the triangle inequality, (30) is obtained.

A.1 Proof of Corollary 1

The proof follows the same steps of the proof of Lemma 2 until (A6).

Substituting $\phi_{i,j}(t) = \sum_{\kappa=1}^{\bar{n}} c_{i,j_\kappa} e^{-h_{i,j_\kappa}t}$ into (A6), we obtain that

$$\begin{aligned} x_i^{(1)}(t) &= \sum_{j=1}^{n-\ell} \left(\sum_{\kappa=1}^{\bar{n}} c_{i,j_\kappa} e^{-h_{i,j_\kappa}t} \right) x_j^{(1)}(0) \\ &\quad + \int_0^t \left(\sum_{j=1}^{n-\ell} \left(\sum_{\kappa=1}^{\bar{n}} c_{i,j_\kappa} e^{-h_{i,j_\kappa}(t-\eta)} \right) \left[\sum_{k=n-\ell+1}^{n} a_{1_{j,k}} \left(x_{k-n+\ell}^{(2)}(0)e^{-\bar{\lambda}\eta} + r_{k-n+\ell}(\eta)\frac{2}{\pi}\tan^{-1}(\bar{\lambda}\eta) \right) \right] \right) d\eta \\ &= \sum_{j=1}^{n-\ell}\sum_{\kappa=1}^{\bar{n}} c_{i,j_\kappa} e^{-h_{i,j_\kappa}t} x_j^{(1)}(0) + \int_0^t \sum_{j=1}^{n-\ell}\sum_{\kappa=1}^{\bar{n}}\sum_{k=n-\ell+1}^{n} c_{i,j_\kappa} e^{-h_{i,j_\kappa}(t-\eta)} a_{1_{j,k}} \left(x_{k-n+\ell}^{(2)}(0)e^{-\bar{\lambda}\eta} + r_{k-n+\ell}(\eta)\frac{2}{\pi}\tan^{-1}(\bar{\lambda}\eta) \right) d\eta \\ &= \sum_{j=1}^{n-\ell}\sum_{\kappa=1}^{\bar{n}} c_{i,j_\kappa} e^{-h_{i,j_\kappa}t} x_j^{(1)}(0) + \sum_{j=1}^{n-\ell}\sum_{\kappa=1}^{\bar{n}}\sum_{k=n-\ell+1}^{n} \Bigg(\int_0^t c_{i,j_\kappa} e^{-h_{i,j_\kappa}(t-\eta)} a_{1_{j,k}} x_{k-n+\ell}^{(2)}(0)e^{-\bar{\lambda}\eta} d\eta \\ &\quad + \int_0^t c_{i,j_\kappa} e^{-h_{i,j_\kappa}(t-\eta)} a_{1_{j,k}} r_{k-n+\ell}(\eta)\frac{2}{\pi}\tan^{-1}(\bar{\lambda}\eta) d\eta \Bigg), \quad i = 1, ..., n-\ell. \end{aligned} \tag{A8}$$

Substituting (19) with $t_0 = 0$ and (A8) in (A3), we get

$$|v_i(t)| = \Bigg| -\sum_{\omega=1}^{n-\ell}\sum_{j=1}^{n-\ell}\sum_{\kappa=1}^{\bar{n}} a_{2_{i,\omega}} c_{\omega j_\kappa} e^{-h_{\omega j_\kappa} t} x_j^{(1)}(0) - \sum_{\omega=1}^{n-\ell}\sum_{j=1}^{n-\ell}\sum_{\kappa=1}^{\bar{n}}\sum_{k=n-\ell+1}^{n} \Bigg(\int_0^t a_{2_{i,\omega}} c_{\omega j_\kappa} e^{-h_{\omega j_\kappa}(t-\eta)} a_{1_{j,k}} x_{k-n+\ell}^{(2)}(0) e^{-\bar{\lambda}\eta} d\eta$$
$$+ \int_0^t a_{2_{i,\omega}} c_{\omega j_\kappa} e^{-h_{\omega j_\kappa}(t-\eta)} a_{1_{j,k}} r_{k-n+\ell}(\eta) \frac{2}{\pi} \tan^{-1}(\bar{\lambda}\eta) d\eta \Bigg) - \sum_{j=n-\ell+1}^{n} a_{2_{i,j}} \left(x_i^{(2)}(0) e^{-\bar{\lambda}t} + \frac{2}{\pi} r_i(t) \tan^{-1}(\bar{\lambda}t) \right)$$
$$- \bar{\lambda} x_{n-\ell+i}(0) e^{-\bar{\lambda}t} + \frac{2}{\pi} \dot{r}_i(t) \tan^{-1}(\bar{\lambda}t) + \frac{2}{\pi} r_i(t) \frac{\bar{\lambda}}{1+\bar{\lambda}^2 t^2} - \bar{s}_i(x(t)) \rho_i \Bigg| \leq M_i, \quad i = 1, \ldots, \ell. \tag{A9}$$

Defining $q_{\omega j_\kappa}(t)$ as

$$q_{\omega j_\kappa}(t) = \int_0^t e^{-h_{\omega j_\kappa}(t-\eta)} e^{-\bar{\lambda}\eta} d\eta = \begin{cases} t e^{-h_{\omega j_\kappa} t}, & \bar{\lambda} = h_{\omega j_\kappa}, \\ \frac{e^{-\bar{\lambda}t} - e^{-h_{\omega j_\kappa} t}}{h_{\omega j_\kappa} - \bar{\lambda}}, & \bar{\lambda} \neq h_{\omega j_\kappa}, \end{cases} \tag{A10}$$

remembering that $\bar{s}_i$ is either 1 or −1, and using the triangle inequality, we can rewrite (A9) as (31).